19. A. Thess *et al.*, *Science* **273**, 483 (1996).
20. J. M. Cowley, P. Nikolaev, A. Thess, R. E. Smalley, *Chem. Phys. Lett.* **265**, 379 (1997).
21. L.-C. Qin, S. Iijima, *Chem. Phys. Lett.* **269**, 65 (1997).
22. R. Saito, G. Dresselhaus, M. S. Dresselhaus, *Physical Properties of Carbon Nanotubes* (Imperial College Press, London, 1998).
23. The chiral angle approaches 30° for each family of nanotube structures in the limit of long transition wavelengths (large diameters).
24. T. Ando, *J. Phys. Soc. Jpn.* **66**, 1066 (2001).
25. M. Ichida, S. Mizuno, Y. Tani, Y. Saito, A. Nakamura, *J. Phys. Soc. Jpn.* **68**, 3131 (1999).
26. Supported by NSF (grant CHE-9900417), the NSF Focused Research Group on Fullerene Nanotube Chemistry (grant DMR-0073046), the NSF Center for Biological and Environmental Nanotechnology (grant EEC-0118007), and the Robert A. Welch Foundation (grants C-0807 and C-0689). Support from NASA (grant NCC 9-77) for development of the HiPco method is also gratefully acknowledged. We thank M. O'Connell and V. Moore for assistance in sample preparation, S. Doorn for Raman spectroscopy, the University of Illinois Materials Research Laboratory for use of facilities, S. Reich for generously sharing computer codes and extended tight binding results before publication, and G. Mele for helpful and stimulating discussions.

24 September 2002; accepted 11 November 2002

Microporous and Photoluminescent Chalcogenide Zeolite Analogs

Nanfeng Zheng,[1] Xianhui Bu,[2] Bing Wang,[1] Pingyun Feng[1]*

Crystalline semiconducting sulfide and selenide zeolite analogs were synthesized that possess four-connected, three-dimensional tetrahedral networks built from tetravalent (M^{4+} = Ge^{4+} or Sn^{4+}, where M = meta) and trivalent (M^{3+} = Ga^{3+} or In^{3+}) cations. Microporous materials were obtained in all four combinations of M^{4+} and M^{3+}, and some of them were thermally stable up to at least 380°C. These materials exhibit framework topologies with pore size ranging from 12 to 24 tetrahedral atoms, high surface area, high framework charge density and ion exchange capacity, and tunable electronic and optical properties.

Microporous materials exemplified by aluminosilicate zeolites have large-scale commercial applications ranging from gas separation to petroleum processing (*1*). For ~50 years, there has been interest in developing porous materials with either novel chemical compositions or new framework topologies because properties and applications of porous materials are intimately related to their compositional and topological features (*2, 3*). In general, the synthesis of new porous materials involves the replacement of tetrahedral atoms (T atoms), such as Al^{3+} or Si^{4+}, in zeolites by other T atoms, such as Ga^{3+}, Ge^{4+}, and P^{5+} (*4*). Resulting oxides are usually insulators and have very limited electro-optic applications.

To expand microporous materials beyond their traditional applications, researchers have found that it is desirable to synthesize microporous semiconducting materials. Crystalline porous semiconductors may find applications in electrocatalysis, photocatalysis, and electrochemical sensor analysis, where size and shape of chemical and biochemical agents are important for selectivity. Analytical applications have the potential for exceptionally high sensitivity because of the preconcentration effect of porous materials through adsorption or ion exchange.

One of the most important goals in developing crystalline porous semiconductors is to generate three-dimensional (3D) frameworks with enhanced thermal stability. Since the late 1980s, research involving porous chalcogenides has received increasing attention with the synthesis of a number of open-framework chalcogenides (*5–10*). When only tetravalent metal cations, such as Ge^{4+} or Sn^{4+}, are used to build chalcogenide frame-

---

[1]Department of Chemistry, University of California, Riverside, CA 92521, USA. [2]Department of Chemistry, University of California, Santa Barbara, CA 93106, USA.

*To whom correspondence should be addressed. E-mail: pingyun.feng@ucr.edu

Table 1. A summary of crystallographic data for selected UCR-20, UCR-21, UCR-22, and UCR-23 structures. Crystal structures were solved from single-crystal data collected at 298 K on a SMART 1000 charge-coupled device diffractometer with Mo Kα. For UCR-21InSnS-AEP, *b* = 16.943 ± 0.003 Å. Standard deviations for *a* and *c* are given by the numbers in parentheses, with the number representing the deviation in the least significant digit(s). TAEA = tris(2-aminoethyl)amine, $C_6H_{18}N_4$; TMDP = 4,4′-trimethylenedipiperidine, $C_{13}H_{26}N_2$; APO = *dl*-1-amino-2-propanol, C_3H_9NO; APP = 1-(3-aminopropyl)-2-pipecoline, $C_9N_2H_{20}$; AEP = 1-(2-aminoethyl)piperazine, $C_6H_{15}N_3$; TOTDA = 4,7,10-trioxa-1,13-tridecanediamine, $C_{10}H_{24}N_2O_3$; AEM = *N*-(2-aminoethyl)morpholine, $C_6H_{14}N_2O$. $R(F) = \Sigma||F_{obs}| - |F_{calc}||/\Sigma|F_{obs}|$ with $F_{obs} > 4.0\sigma(F)$.

Structure	Framework composition	Space group	*a* (Å)	*c* (Å)	*R*(*F*)
UCR-20GaGeS-TAEA	$Ga_{2.67}Ge_{1.33}S_8$	$-4 \rightarrow \bar{4}$	20.9352(15)	20.9352(15)	7.21
UCR-20GaSnS-TMDP	$Ga_{1.80}Sn_{2.20}S_8$	$-4 \rightarrow \bar{4}$	21.5404(17)	21.5404(17)	5.54
UCR-20InGeS-TMDP	$In_{3.00}Ge_{1.00}S_8$	$-4 \rightarrow \bar{4}$	21.734(2)	21.734(2)	7.61
UCR-20InSnS-TMDP	$In_{2.50}Sn_{1.50}S_8$	$-4 \rightarrow \bar{4}$	22.1906(18)	22.1906(18)	7.61
UCR-20GaGeSe-TMDP	$Ga_xGe_{4-x}Se_8$	$-4 \rightarrow \bar{4}$	21.893(2)	21.893(2)	7.40
UCR-21GaGeS-APO	$Ga_{3.30}Ge_{0.70}S_8$	$-4 \rightarrow \bar{4}$	11.1414(15)	19.405(4)	4.18
UCR-21GaSnS-TAEA	$Ga_{2.32}Sn_{1.68}S_8$	$-4 \rightarrow \bar{4}$	11.6915(19)	19.898(5)	4.46
UCR-21InGeS-APP	$In_{1.84}Ge_{2.16}S_8$	$-4 \rightarrow \bar{4}$	11.5313(15)	19.936(4)	6.94
UCR-21InSnS-AEP	$In_xSn_{4-x}S_8$	$-4 \rightarrow \bar{4}$	13.379(2)	25.973(5)	6.48
UCR-21GaSnSe-TAEA	$Ga_{2.47}Sn_{1.53}Se_8$	$-4 \rightarrow \bar{4}$	12.5373(19)	20.564(4)	6.04
UCR-22GaGeS-AEP	$Ga_{3.33}Ge_{0.67}S_8$	$-4 \rightarrow \bar{4}$	22.532(2)	39.954(5)	6.23
UCR-22GaSnS-AEP	$Ga_{2.13}Sn_{1.87}S_8$	$-4 \rightarrow \bar{4}$	22.935(2)	40.985(6)	5.51
UCR-22InGeS-AEP	$In_{2.69}Ge_{1.31}S_8$	$-4 \rightarrow \bar{4}$	22.9078(12)	41.490(3)	5.82
UCR-22GaSnSe-TOTDA	$Ga_{1.73}Sn_{2.27}Se_8$	$-4 \rightarrow \bar{4}$	23.841(3)	42.555(7)	6.83
UCR-23GaGeS-AEM	$Ga_{2.67}Ge_{1.33}S_8$	$-4 \rightarrow \bar{4}$	21.638(3)	11.209(2)	5.43
UCR-23GaSnS-AEM	$Ga_{2.29}Sn_{1.71}S_8$	$-4 \rightarrow \bar{4}$	22.169(3)	11.3168(18)	5.68
UCR-23InGeS-AEM	$In_{1.84}Ge_{2.16}S_8$	$-4 \rightarrow \bar{4}$	22.153(3)	11.3435(18)	6.79

works, there is a strong tendency to form non-3D structures. Early attempts to prepare 3D microporous chalcogenides depended primarily on the use of mono- or divalent cations (e.g., Mn^{2+}) to join together chalcogenide clusters, such as $Ge_4S_{10}^{4-}$ (*11–13*). These low-charged metal sites could decrease the framework stability. The destabilizing effect of divalent cations (e.g., Co^{2+}, Mn^{2+}) in porous aluminophosphates is well known (*14–16*). Recently, indium chalcogenides with or without the incorporation of mono- or divalent cations have been reported to have highly open architecture (*6, 9, 17, 18*), but these materials usually collapse at temperatures that are <300°C. To enhance framework stability and to develop thermally stable porous semiconductors, we adapted the stability rule for zeolite synthesis, which states that stability requires that a Si^{4+}/Al^{3+} ratio is not less than 1. We found that stability in the metal chalcogenides also requires a M^{4+}/M^{3+} ratio range. The range of the M^{4+}/M^{3+} ratio for materials synthesized in this work is between 0.2 and 1.2.

We synthesized a large family of chalcogenide zeolite analogs by simultaneous triple substitutions of O^{2-} with S^{2-} or Se^{2-}, Si^{4+} with Ge^{4+} or Sn^{4+}, and Al^{3+} with Ga^{3+} or In^{3+}. All four possible M^{4+}/M^{3+} combinations (Ga/Ge, Ga/Sn, In/Ge, and In/Sn) could be realized, resulting in four zeolite-type topologies. More than 12 distinct framework materials were synthesized by changing either the topological types or the framework composition (Table 1) (*19, 20*). The actual number of as-synthesized compounds is substantially greater than that included in Table 1 because of the large variations in extra-framework organic components (table S1). In addition, new forms can be created by replacing organic components with inorganic cations through ion exchange. The distribution of M^{4+} and M^{3+} in the framework of these materials is random. In addition to single crystals and polycrystalline powders, thin films were grown over some substrates, such as graphite electrodes under hydrothermal conditions (fig. S1).

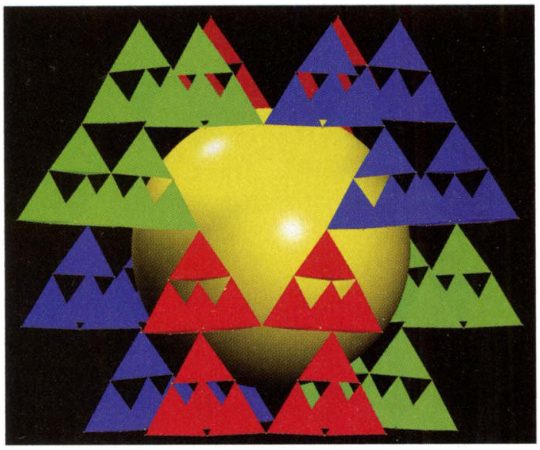

Fig. 1. A sodalite cage decorated with M_4X_{10} (M = Ga/Ge, Ga/Sn, In/Ge, and In/Sn; X = S and Se) clusters in UCR-20. Colors are arbitrary and represent different chemical units.

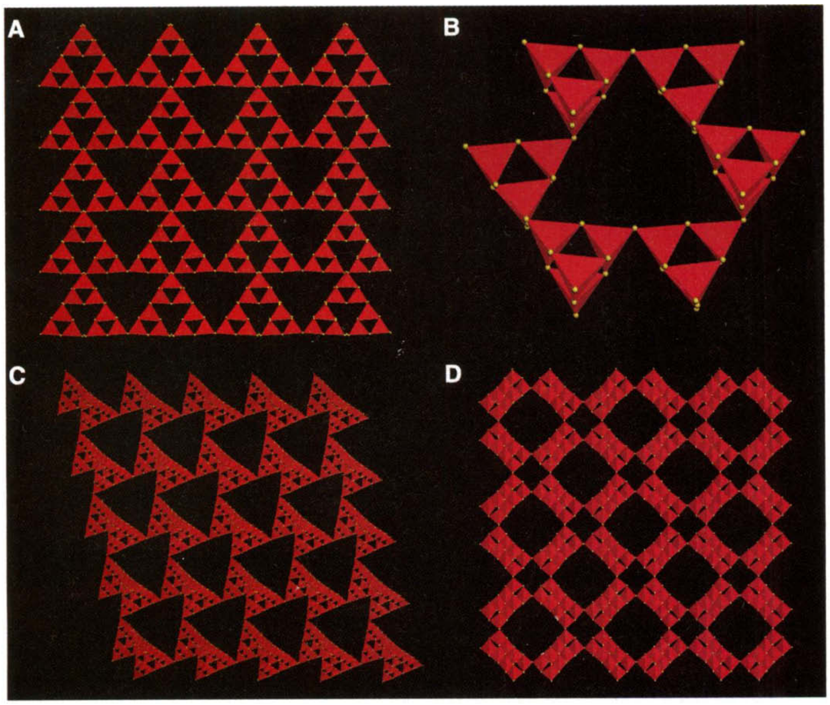

Fig. 2. (**A**) The 3D M_4X_{10} decorated sodalite framework in UCR-20. (**B**) Six M_4X_{10} clusters are joined into a six-membered ring in UCR-21 with the decorated cubic ZnS framework. (**C**) The 3D framework of UCR-22 with the cubic ZnS–type topology decorated with the coreless T4 supertetrahedral cluster ($M_{16}X_{34}$). Only one lattice set in UCR-22 is shown. (**D**) The 3D framework of UCR-23 with the decorated CrB_4 topology projected down the 16-ring channels. Small yellow spheres represent sites of sulfur atoms; metal cations (Ge^{4+}, Ga^{3+}, Sn^{4+}, and In^{3+}) are located at the center of every red tetrahedron.

On the basis of structural type, these materials are classified into four families: UCR-20, UCR-21, UCR-22, and UCR-23. Each number refers to a series of materials with the same framework topology but with different chemical compositions in either framework or extra-framework components. For example, UCR-20 can be made in all four M^{4+}/M^{3+} combinations, giving rise to four subfamilies: UCR-20GaGeS, UCR-20GaSnS, UCR-20InGeS, and UCR-20InSnS. The number of subfamilies doubles if selenides are included. An individual compound is specified when both the framework composition and the type of extra-framework species are specified (e.g., UCR-20GaGeS-AEP).

One of the most important features of the structures reported here is the diversity of their framework compositions. The large variety of chemical compositions makes it possible to tune physical properties, such as band gap, luminescence, pore size, surface area, ion exchange, and chemical stability. Compared to other open-framework chalcogenides, such as germanium sulfides or indium sulfides, these chemical systems are particularly intriguing because of their direct relation to aluminosilicate zeolites in both composition and structure. All of these materials have four-connected, 3D zeolite-type connectivity. Also like zeolites, they are all built from tetravalent and trivalent cations with a general framework composition of AB_2, where A is a tetrahedral cation (Ga, In, Ge, and Sn) and B is a bicoordinated anion (S and Se). In some of these materials that have unusually low M^{4+}/M^{3+} ratios of ~0.20, a very large negative charge develops on the framework, which should be desirable in applications such as gas separation and ion exchange, where a high concentration of charge-balancing cations is beneficial.

The extra-large pore size and "3-rings" (three T atoms in a ring) are two other striking features. UCR-22 and UCR-23 have an uncommon pore size consisting of 24 and 16

T atoms, respectively, whereas UCR-20 and UCR-21 are both large-pore (12 T atoms) materials. These inorganic frameworks are strictly four-connected 3D networks commonly used for the systematic description of zeolite frameworks. Unlike known zeolite structure types, a key structural feature is the presence of the adamantane cage–shaped building unit, M_4S_{10} (*21*). The M_4S_{10} unit consists of four 3-rings fused together. The presence of 3-rings is one of the most desirable features in a zeolite-type topology because it helps to generate a low-density framework (*22*). For materials reported here, the framework density (defined as the number of T atoms in 1 nm^3) ranges from 4.4 to 6.5 (table S1).

Although these chalcogenides are strictly zeolite-type tetrahedral frameworks, it is possible to view them as decoration of even simpler tetrahedral frameworks. "Decoration" refers to the replacement of a single atom by a multiatom cluster having the same connectivity pattern (*21*). Here, each M_4S_{10} unit can be treated as a large artificial tetrahedral atom. With this description, UCR-20 has the decorated sodalite-type structure, in which a tetrahedral site in a regular sodalite net is replaced with a M_4S_{10} unit (Figs. 1 and 2A). UCR-21 has the decorated cubic ZnS–type structure (Fig. 2B). Open-framework materials with the cubic ZnS–type lattice usually form two or more interpenetrating sublattices; however, UCR-21 is non-interpenetrating and non-centrosymmetric. UCR-23 has the decorated CrB_4-type network, in which tetrahedral boron sites are replaced with M_4S_{10} units (Fig. 2D). The M_4S_{10} cluster is a special decoration unit because all of its sulfur sites are bicoordinated. As a result, a four-connected, 3D tetrahedral net decorated with M_4S_{10} units remains a zeolite-type four-connected, 3D net.

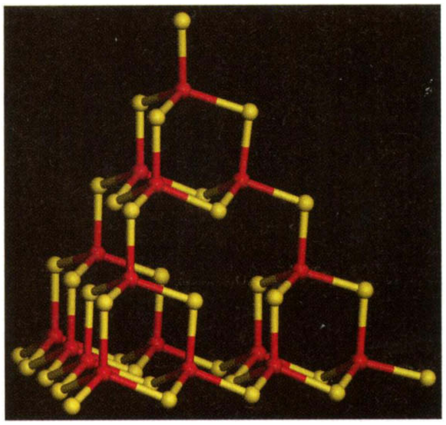

Fig. 3. The coreless pseudo-T4 supertetrahedral cluster ($M_{16}X_{34}$) in UCR-22. The decoration unit in UCR-22 is $M_{16}X_{34}$, which is different from that (M_4X_{10}) in UCR-20, UCR-21, and UCR-23. Yellow spheres represent sulfur or selenium sites; red spheres represent metal sites.

An interesting cluster, $M_{16}X_{34}$ (X = S or Se), occurs in UCR-22. This cluster is constructed from four M_4S_{10} cage units sharing corner S^{2-} sites (Fig. 3). It resembles a regular supertetrahedral T4 cluster (general formula $M_{20}X_{35}$), except that the central sulfur site and its four adjacent metal sites are not occupied (*23, 24*). A complete T4 cluster contains a single sulfur core atom. When this core sulfur atom is missing, all of its neighboring metal sites must also be left unoccupied because three-coordinated metal cations (Ga^{3+}, In^{3+}, Ge^{4+}, and In^{4+}) in these materials are not stable. Such a coreless feature ensures that all cations have tetrahedral coordination and all anions have bicoordination, an essential characteristic in a four-connected, 3D zeolite-type structure. If each coreless T4 cluster is treated as a large pseudo-tetrahedral atom, the inorganic framework consists of two interpenetrating, cubic ZnS–type lattices (Fig. 2C).

The M^{4+}/M^{3+} sulfides reported have substantially improved thermal and mechanical stability over those of many previously reported, crystalline open-framework sulfides, such as indium sulfides. Selected samples (e.g., UCR-20GaGeS-AEP, UCR-20GaGeS-TAEA, UCR-20InGeS-TMDP, UCR-20InSnS-TMDP, UCR-21GaGeS-AEM, UCR-22InGeS-AEP, UCR-22GaSnS-AEP, and UCR-23GaGeS-AEM) maintained their structural and mechanical integrity when heated in air at 300°C for 1 hour. In all cases, despite a significant weight loss of up to ~20%, the single-crystal quality was retained, as demonstrated by single-crystal x-ray diffraction. Powder x-ray diffraction shows that some of these compounds (e.g., UCR-20GaGeS-TAEA) are stable at 380°C in argon. A higher thermal stability (at least to 420°C) is observed for the Cs^+-exchanged UCR-20GaGeS-TAEA under vacuum.

Direct calcination of as-synthesized samples can remove a sizable fraction of extra-framework organic components. In one experiment, ~77% of nitrogen and ~81% of hydrogen were removed from UCR-20GaGeS-TAEA by direct calcination at 350°C in nitrogen (*20*). However, the coke formation makes the removal of carbon more difficult than the removal of nitrogen and hydrogen. About 39% of carbon

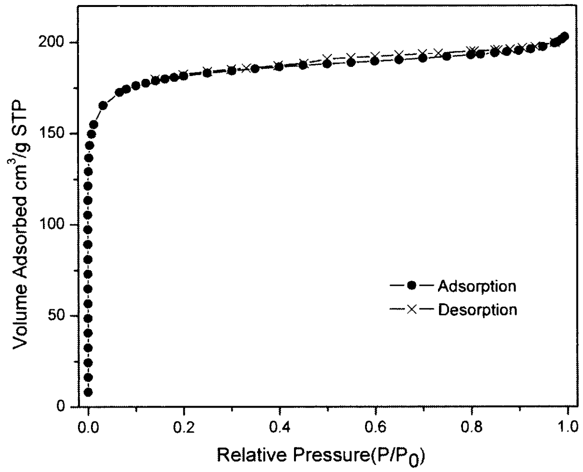

Fig. 4. Nitrogen adsorption and desorption isotherms measured at 77 K on a Micromeritics ASAP 2010 Micropore Analyzer for the Cs^+-exchanged UCR-20GaGeS-TAEA. The ion exchange was performed at 373 K for 60 hours and then dried at 353 K for 2 hours. Before the measurement, the sample was degassed at 373 K for 6 hours and then at room temperature for 16 hours. STP, standard temperature and pressure.

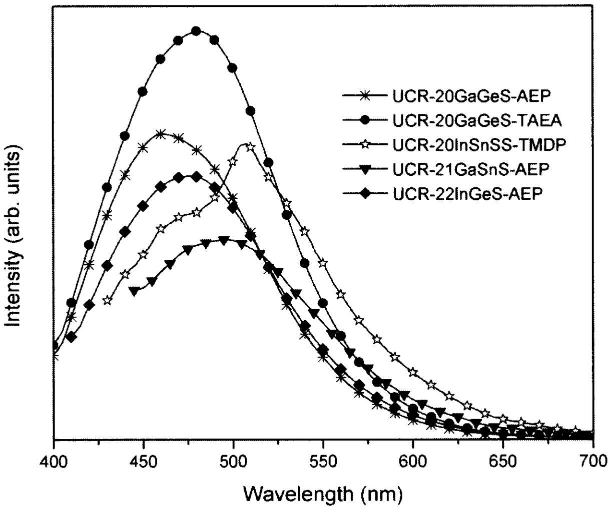

Fig. 5. Photoluminescent emission spectra of selected compounds.

was removed from UCR-20GaGeS-TAEA in the same experiment.

Ion exchange with NH_4^+ followed by calcination makes it possible to remove extra-framework species at temperatures as low as 100°C. For NH_4^+-exchanged UCR-20GaGeS-TAEA, a thermogravimetric analysis showed that the weight loss of 17.2% occurred between 80° and 150°C, which is much less than the temperature range needed for the direct calcination of the as-synthesized amine-containing sample (300° to 360°C). An x-ray powder diffraction shows that the sample remains highly crystalline after the calcination of the NH_4^+-exchanged sample at 180°C under argon atmosphere (fig. S2).

In addition to NH_4^+, these materials undergo ion exchange with many mono- and divalent metal cations. For example, upon exchange with Cs^+ ions, the percentages of C, H, and N in UCR-20GaGeS-TAEA were dramatically reduced (*20*). Yet, like the original sample, the exchanged sample remains highly crystalline. The Cs^+-exchanged UCR-20GaGeS-TAEA exhibits the type I isotherm characteristic of a microporous solid (Fig. 4). This sample has a high Langmuir surface area of 807 m^2/g and a micropore volume of 0.23 cm^3/g, despite the presence of much heavier elements (Cs, Ga, Ge, and S), as compared to the elements present in aluminosilicate zeolites. The median pore diameter calculated with the Horvath-Kawazoe method is 9.5 Å, 14% larger than that for Molecular Sieve Type 13X (8.2 Å) determined under the same experimental conditions.

These sulfides are also strongly photoluminescent and can be excited with wavelengths from 360 to 420 nm. The emission maximum occurs in the range from 460 to 508 nm (Fig. 5). For example, UCR-20GaGeS-TAEA strongly luminesces at 480 nm when excited at 370 nm. The general trend is that materials with heavier elements are excited and luminesce at a longer wavelength.

References and Notes

1. M. E. Davis, *Nature* **417**, 813 (2002).
2. Ch. Baerlocher, W. M. Meier, D. H. Olson, *Atlas of Zeolite Framework Types* (Elsevier, Amsterdam, 2001).
3. A. Corma, M. J. Diaz-Cabanas, J. Martinez-Triguero, F. Rey, J. Rius, *Nature* **418**, 514 (2002).
4. A. K. Cheetham, G. Ferey, T. Loiseau, *Angew. Chem. Int. Ed.* **38**, 3268 (1999).
5. R. L. Bedard, S. T. Wilson, L. D. Vail, J. M. Bennett, E. M. Flanigen, in *Zeolites: Facts, Figures, Future. Proceedings of the 8th International Zeolite Conference*, P. A. Jacobs, R. A. van Santen, Eds. (Elsevier, Amsterdam, 1989), pp. 375–387.
6. C. L. Cahill, J. B. Parise, *J. Chem. Soc. Dalton Trans.* **2000**, 1475 (2000).
7. S. Dhingra, M. G. Kanatzidis, *Science* **258**, 1769 (1992).
8. R. W. J. Scott, M. J. MacLachlan, G. A. Ozin, *Curr. Opin. Solid State Mater. Sci.* **4**, 113 (1999).
9. H. Li, A. Laine, M. O'Keeffe, O. M. Yaghi, *Science* **283**, 1145 (1999).
10. H. Ahari, A. Lough, S. Petrov, G. A. Ozin, R. L. Bedard, *J. Mater. Chem.* **9**, 1263 (1999).
11. O. M. Yaghi, Z. Sun, D. A. Richardson, T. L. Groy, *J. Am. Chem. Soc.* **116**, 807 (1994).
12. K. Tan, A. Darovsky, J. B. Parise, *J. Am. Chem. Soc.* **117**, 7039 (1995).
13. C. L. Bowes *et al.*, *Chem. Mater.* **8**, 2147 (1996).
14. E. M. Flanigen, in *Introduction to Zeolite Science and Practice*, H. van Bekkum, E. M. Flanigen, J. C. Jansen, Eds. (Elsevier, New York, 1991), pp. 13–34.
15. P. Feng, X. Bu, G. D. Stucky, *Nature* **388**, 735 (1997).
16. X. Bu, P. Feng, G. D. Stucky, *Science* **278**, 2080 (1997).
17. X. Bu, N. Zheng, Y. Li, P. Feng, *J. Am. Chem. Soc.* **124**, 12646 (2002).
18. C. Wang, X. Bu, N. Zheng, P. Feng, *J. Am. Chem. Soc.* **124**, 10268 (2002).
19. An example of a typical synthesis condition with the preparation of UCR-20GaGeS-TAEA is as follows. Gallium metal (82.7 mg), germanium oxide (109.1 mg), sulfur (222.1 mg), and tris(2-aminoethyl)amine (2.1719 g) were mixed in a Teflon-lined stainless steel autoclave for ~20 min. The vessel was then sealed and heated at 190°C for 6 days. The autoclave was subsequently cooled to room temperature. Transparent, pale yellow crystals were obtained with a yield of ~67%.
20. Materials and methods, results of the elemental analysis, details of the thin-film structure, and x-ray powder diffraction data are available on *Science* Online. Crystallographic data (excluding structure factors) have been deposited with the Cambridge Crystallographic Data Center (CCDC) as supplementary publications CCDC 197105 through 197126 and CCDC 197207 through 197214.
21. M. O'Keeffe, M. Eddaoudi, H. Li, T. Reineke, O. M. Yaghi, *J. Solid State Chem.* **152**, 3 (2002).
22. G. O. Brunner, W. M. Meier, *Nature* **337**, 146 (1989).
23. H. Li, J. Kim, T. L. Groy, M. O'Keeffe, O. M. Yaghi, *J. Am. Chem. Soc.* **123**, 4867 (2001).
24. C. Wang *et al.*, *J. Am. Chem. Soc.* **123**, 11506 (2001).

25. Supported by NSF (grant CHE-0213310) and the Air Force Office of Scientific Research (for a grant to purchase an x-ray powder diffractometer). We thank H. Luo, S. Li, and Y. Yan for their assistance with adsorption measurements.

Supporting Online Material

www.sciencemag.org/cgi/content/full/298/5602/2366/DC1

Materials and Methods

Figs. S1 and S2

Table S1

23 September 2002; accepted 12 November 2002

Mass-Independent Sulfur of Inclusions in Diamond and Sulfur Recycling on Early Earth

J. Farquhar,[1] B. A. Wing,[1] K. D. McKeegan,[2] J. W. Harris,[3] P. Cartigny,[4] M. H. Thiemens[5]

Populations of sulfide inclusions in diamonds from the Orapa kimberlite pipe in the Kaapvaal-Zimbabwe craton, Botswana, preserve mass-independent sulfur isotope fractionations. The data indicate that material was transferred from the atmosphere to the mantle in the Archean. The data also imply that sulfur is not well mixed in the diamond source regions, allowing for reconstruction of the Archean sulfur cycle and possibly offering insight into the nature of mantle convection through time.

An understanding of the nature of the source materials for diamonds would provide important insights into large-scale geophysical processes. For example, elemental and isotopic data have been used to argue that diamonds and their inclusions are relics of subducted crustal materials (*1–9*), but alternate explanations such as mantle fractionation processes or relict primordial heterogeneity are plausible (*10–15*). Here we report mass-independently fractionated {anomalous $\Delta^{33}S = \delta^{33}S - 1000 \times [(1 + \delta^{34}S/1000)^{0.515} - 1]$} (*16*) sulfur isotope compositions for syngenetic sulfide inclusions in diamond from the Orapa kimberlite pipe, Kaapvaal-Zimbabwe craton, Botswana. We also discuss the implications of $\Delta^{33}S$ as an almost perfect tracer of the exchange between Earth's geochemical reservoirs because of its exclusive origin through atmospheric photochemistry and its preservation through subsequent mass-dependent fractionation processes.

The Orapa kimberlite pipe is located within the Magondi belt, a region of thick (150 to 225 km) crust along the western margin of the Kaapvaal-Zimbabwe craton, which is considered to be the surface manifestation of the Proterozoic reactivation of the Kaapvaal-Zimbabwe craton (*17–19*). Diamonds from Orapa are predominantly eclogite types and have a wide range of $\delta^{13}C$ values [(–26 to –3 per mil (‰)], $\delta^{15}N$ values (–10 to +6‰), nitrogen contents [(8 to 3450 parts per million (ppm)], and nitrogen aggregation states (a 0 to 95% degree of association) (*1*, *12*, *20*). Silicate and sulfide inclusions from these diamonds have at least two distinct ages (*1*, *19*): an Archean population of 2.9 Ga and a Proterozoic population of 1.0 billion years ago (Ga) (*1*, *19*). The sulfide inclusions also have

---

[1] Earth System Science Interdisciplinary Center and Department of Geology, University of Maryland, College Park, MD 20742, USA. [2] Department of Earth and Space Sciences, University of California, Los Angeles, CA 90095, USA. [3] Division of Earth Sciences, Gregory Building, University of Glasgow, Glasgow, G12 8QQ, UK. [4] Laboratoire de Géochimie des Isotopes Stables, Université Paris VII, Institut de Physique du Globe de Paris, 75252 Paris Cedex 05, France. [5] Department of Chemistry and Biochemistry, University of California, San Diego, La Jolla, CA 92093, USA.